

Coupling and control in coherently driven and asymmetrically synchronized hybrid electron-nuclear spin system

V. Berc^{1,2,a}

¹ Institute of Nuclear Sciences Vinca, PO Box 522, 11001 Belgrade, Serbia

² University of Belgrade, St. Trg 1, 11000 Belgrade, Serbia

Received 17 June 2015 / Received in final form 11 January 2016
Published online 29 February 2016

Abstract. We study the coupling and control adaptation of a hybrid electron-nuclear spin system using the laser mediated proton beam in MeV energy regime. The asymmetric control mechanism is based on exact optimization of both: the measure of exchange interaction and anisotropy of the hyperfine interaction induced in the resonance with optimal channeled protons (CP) superfocused field, allowing manipulation over arbitrary localized spatial centers while addressing only the electron spin. Using highly precise and coherent proton channeling regime we have obtained efficient pulse shaping separator technique aimed for spatio-temporal engineering of quantum states, introducing a method for control of nuclear spins, which are coupled via anisotropic hyperfine interactions in isolated electron spin manifold, without radio wave (RW) pulses. The presented method can be efficiently implemented in synchronized spin networks with the purpose to facilitate preservation and efficient transfer of experimentally observed quantum particle states, contributing to the overall background noise reduction.

1 Introduction

The ability to generate, control and transfer the atom-photon quantum correlation between light-matter interfaces [1–6] represents the central topic of recent developments toward the fields of complex systems, information theory and quantum information processing. However, in the presence of noise it is hard to produce, precisely assess and to classify the dynamics of quantum states according to their entanglement properties [7]. Motivated by the fact that the mixed state quantum property, as a robust entanglement resource, allows the possibility of employing a noisy environment, using a recently introduced framework [8–10] we investigate the hybrid proton mediated electron-nuclear spin dynamics in a nanocrystal channel of diamond symmetry, performing combined theoretical and experimental study.

In contrast to recently proposed doped silicon architectures [11–13], where the main problem of decoherence in view of the temperature dependent spin-boson and

^a e-mail: bervesn@gmail.com; vberec@vin.bg.ac.rs

temperature independent spin-spin mechanisms predominates, a long quantum coherence time of 25 seconds for ^{29}Si nuclear spins at room temperature as one of the main criteria for nuclear spin to be utilized as a memory qubit [14] is explored in this study using isotopically highly abundant pure silicon nanocrystal, demonstrating at the same time advantage of ^{29}Si nuclear spins in coherent quantum interactions and quantum feedback control [15], and highlighting their excellent characteristics for solid state qubits. In fact, one of the most prominent tasks of secure quantum information processing (QIP) is the frame synchronization applied to qubit rotations on time scales below the spin coherence time. In the quantum domain the actual logical qubit of information can be processed in weak measurement setting as a physical qubit which binds light-matter interface, using quantum feedback protocols for universal control.

After introducing the analytical model, in Sect. 3 we demonstrate that adaptive control of nuclear spin states can be obtained by combinations of switching and time delay mechanisms, manipulating the state of the electron spin defined by its two eigenstates by sequences of π pulses in specific time frame. Successive flipping of the state of electron spin consequently affects the nuclear spin dynamics, which is encoded in quantization axis and the precession frequency relative to this axis, by producing nutation of the nuclear spin around the new quantization axis during each flip. By generating the series of time scaled switchings of electron spin flips followed by specific delays we demonstrate universal control of nuclear spin rotation. Presented switching regime of control of nuclear spin evolution (obtained in electron spin manifold) represents direct implementation of control theory [16] in QIP. Instead of rf field we use CP-modulated beam to produce the nuclear spin hyperpolarization, which extends the electron spin coherence time in nanocrystal, allowing spin qubit manipulation on much faster time scales than the spin coherence time [17], which in turn reduces relaxation losses.

The experimental protocol for atom-photon entangled states established via $\langle 100 \rangle$ nanosilicon interface, is further described in Sect. 3.1. Initially, the system containing two nuclear spins (^1H and ^{29}Si nuclear spin) is coupled via anisotropic hyperfine interaction with electron spin in a ground state. This state is further laser-excited to a metastable triplet. After the initial preparation, the system provides all requirements for exploration of the hybrid nuclear-electron [18,19] spin manipulations which can be mediated by a proton spin in conjunction with hyperfine-transient electron spin (via dynamic nuclear polarization [20]), using a combination of 2 MeV energy polarized channeled proton beam pulses driven in picosecond scale, and a laser excitation at the wavelength of 221.7 nm [21]. The 2 MeV energy establishes acceleration of the spin interactions due to nuclear spins long coherence lifetimes [22] and compensates weak polarization of the nuclear spins, thus overcomes the spin decoherence limit imposed by the noisy environment. The preparation of the initial state considers the hyperfine coupling induced by the proton beam pulses in a 92 nm thick nanosilicon crystal target following the experimental conditions introduced in [9].

2 Model

In order to determine the appropriate coupling parameters and quantity measure of maximal correlation between the nuclear spins states, i.e., the concurrence [23] and entanglement of formation [24], we constructed the entangled state of subsystems A, B over the subspace $V \subset H_A \otimes H_B$. The bipartite state is initialized by two linearly independent non-orthogonal states $|M\rangle_A = \sum_{i_1 \dots i_m} \psi_{M i_1 \dots i_m} |i_1\rangle \dots |i_m\rangle$ and $|L\rangle_B = \sum_{j_1 \dots j_m} \psi_{L j_1 \dots j_m} |j_1\rangle \dots |j_m\rangle$ that span a two dimensional subspaces A and B of Hilbert spaces: H_A, H_B . These two non-orthogonal quantum states [25–27] have

nonzero inner product $\langle \psi_M | i \rangle_A \neq 0, \langle \psi_L | j \rangle_B \neq 0$, where $|\psi_M\rangle_A$ and $|i\rangle_A$ are normalized states of subsystem A , while $|\psi_L\rangle_B$ and $|j\rangle_B$ denote normalized states for subsystem B , respectively. The initial bipartite quantum state then corresponds to:

$$|\Psi\rangle = \frac{1}{N} [\mu |\psi_M\rangle_A \otimes |\psi_L\rangle_B + \xi |i\rangle_A \otimes |j\rangle_B], \quad (1)$$

where μ is the maximal overlap measure, defined for subsystems A, B [26], and the normalization constant is given by

$$N^2 = |\mu|^2 + |\xi|^2 + 2\text{Re}(\mu^* \xi^* p_1 p_2), \quad p_1 = \langle \psi_M | i \rangle, \quad p_2 = \langle j | \psi_L \rangle. \quad (2)$$

The presence of entanglement is first determined by the concurrence $C = |\langle \Psi | \tilde{\Psi} \rangle|$ [28] of the initial state, Eq. (1). In the Pauli basis representation, where σ_y denotes the Pauli spin matrix, the concurrence is:

$$C = |\langle \Psi | \sigma_y \otimes \sigma_y | \Psi \rangle|, \quad (3)$$

defining the overlap between the initial state $|\Psi\rangle$ (Eq. (1)) and the spin-flipped state $|\tilde{\Psi}\rangle = -\sigma_y \otimes \sigma_y |\Psi\rangle$ [28], where the obtained joint (flipped) state defines a rotation about the y -axis corresponding to the effect of the rotating field B_1 in nuclear spin manifold. In particular, following the ideas of Caves et al. [28], the problem of evaluating the entanglement via optimum concurrence from Eq. (3) was shown to be equivalent to that of adjusting the resonance of the external magnetic field where the obtained joint (flipped) state defines a rotation about the y -axis corresponding to sinusoidal oscillating component of dynamic field B_1 which induces precessions of magnetization transversal M_x and longitudinal M_z component [20], directly affecting the spin relaxation times T_2 and T_1 , respectively. In order to further assess the entanglement for generated ion-atom mixed state (obtained in $S-T_+$ basis), it is necessary to represent the (average) concurrence as a minimum taken over all pure-state decompositions [28] of Eq. (1):

$$C_{\min} = \inf \left(\sum_j p_j C(|\psi_j\rangle) \right) = |\text{tr}(\rho \sigma_y \otimes \sigma_y)|, \quad (4)$$

where $|\psi_j\rangle$ are defined in real-vector-space, exclusively. In particular case for generated mixed state $\rho = \frac{1}{2}(|\Phi^+\rangle\langle\Phi^+| + |\Psi^-\rangle\langle\Psi^-|)$, C_{\min} measures the total detection reliability of readable singlet-triplet entangled mixed state realizations:

$$\rho = \frac{1}{4}(I \otimes I + \sigma_y \otimes \sigma_y), \quad (5)$$

which are maximally entangled according to real vector space and represent an equal mixture of the two pure entangled states: $\frac{1}{\sqrt{2}}(|01\rangle - |10\rangle)$ and $\frac{1}{\sqrt{2}}(|00\rangle + |11\rangle)$. In particular case, in contrast to the product decomposition of mixed state $\rho = \frac{1}{2}(|\Phi^+\rangle\langle\Phi^+| + |\Psi^-\rangle\langle\Psi^-|)$, which can be rewritten as $\rho = \frac{1}{2}(|\chi^+\rangle\langle\chi^+| + |\chi^-\rangle\langle\chi^-|)$, where $|\chi^+\rangle = \frac{1}{\sqrt{2}}(|\Phi^+\rangle + i|\Psi^-\rangle) = \frac{1}{2}((|0\rangle - i|1\rangle) \otimes (|0\rangle + i|1\rangle))$, and $|\chi^-\rangle = \frac{1}{\sqrt{2}}(|\Phi^+\rangle - i|\Psi^-\rangle) = \frac{1}{2}((|0\rangle + i|1\rangle) \otimes (|0\rangle - i|1\rangle))$, ρ in form of Eq. (5) is indeed maximally entangled state in the real-vector-space where its concurrence (Eq. (4)) obtains a maximal value [29]: $C_{\min} = |\text{Tr}(\rho \sigma_y \otimes \sigma_y)| = \frac{1}{4} \text{Tr}((\sigma_y \otimes \sigma_y)(\sigma_y \otimes \sigma_y)) = 1$

Accordingly, the entanglement of formation, E_F [24, 29], is dependable on obtained mixed state that corresponds to a density matrix: $\rho \in \mathcal{K}(H_A \otimes H_B)$, and spans a two dimensional Hilbert space over subsets A and B as:

$$E_F(\rho) = \inf_{d \in D_\rho} \sum_k p_k H_{\min}(\rho_{AB}), \quad (6)$$

where, the minimization is determined via von Neumann minimal conditional entropic measure, H_{min} , and given over domain D_ρ which represents the set of all realizable mixed states. The latter relation can be applied to the process of elementary mixtures for Werner quantum system (spanned over subspace: $V \subset H_A \otimes H_B$ which employs two qubits: A and B). Namely, in the past years it was believed that Werner states [30] possess the most entanglement for a certain level of mixedness [30]. Depending on the singlet weight p , Werner states may be entangled $p > 1/3$, or separable for $p \leq 1/3$ [30]. Here employed, Werner state represent a figure of merit in a modeling of a (de)coherence process which affects the singlet state dynamics along a noisy channel [1]. Correspondingly, it is used to model a subsequent induced ion-photon excitation (see Sect. 3).

3 Discussion and results

The swift 2 MeV energy protons are confined under the axial channeling regime (when the channeled proton trajectory corresponds to oscillatory motion) and strongly localized between adjacent atomic rows. We have used the axial channeling configuration in order to increase the confinement effect over ion trajectories, allowing them to be efficiently captured within one single channel [31]. In particular, we have used the 92 nm thick silicon nanocrystal to capture proton oscillatory motion between four neighboring atomic rows according to diamond lattice fcc symmetry of Si $\langle 100 \rangle$ channel, as shown in Fig. 1 (top).

The incident proton beam is tilted relative to z -axis, i.e., low index axis of Si nanocrystal, for the specific values of angles below critical angle for channeling [31]. The gap between the two Si lattice sites represents the nanocrystal cavity [32,33]. Four nanocrystal atomic planes, which perpendicularly intersect the corresponding atomic rows of $\langle 100 \rangle$ channel, interact with CP field [9] producing a gap smaller than the half of the planar oscillation wavelength of the proton beam (its coherence length). Nanocrystal planes act as a mirror that deflects and reverses the transverse motion of the ion trajectories, forming the resonant cavity conditions similar to an X rays resonator [33]. Based on theoretical study [34] that a high efficient mirror for charged particles can be generated by an ultrathin crystal, which is tilted relative to the direction of the incident beam for typical angles smaller than $\psi_c = 6.09$ mrad, recent study [9] exposed a method for nonlinear control of channeled ions, guided via coherent interactions in silicon crystal of thickness parameter smaller than 100 nm. More recently, axial confinement produced by the ultrathin silicon ion channeling was experimentally confirmed for nonrelativistic protons, focused through a 55 nm thick [001] Si membrane [35]. It was shown that the transverse phase space can be populated by channeled ion trajectories, allowing an effective resource of transversely polarized particles [36,37].

Here we consider a structure comprising two main Hamiltonian components: the ion-atom confinement potential, acting inside the silicon nanocrystal cavity, and the internal-spin-Hamiltonian. In order to describe the system properties and dynamics of the continuum ion-atom interaction potential in the nanocrystal, we include the Hamiltonian governing the oscillatory motion of ions

$$H = (1/2) m (p_\perp^2 + U(r)) = E (\psi_x^2 + \psi_y^2) + U(r), \quad E_\perp = E\psi^2 + U(r), \quad (7)$$

where E is ion incident energy, E_\perp and p_\perp denote ion transverse energy and momentum, ψ_x and ψ_y are x and y components of scattering small angle with respect to the low index channel axis. The proton trajectories are obtained in the Moliere's

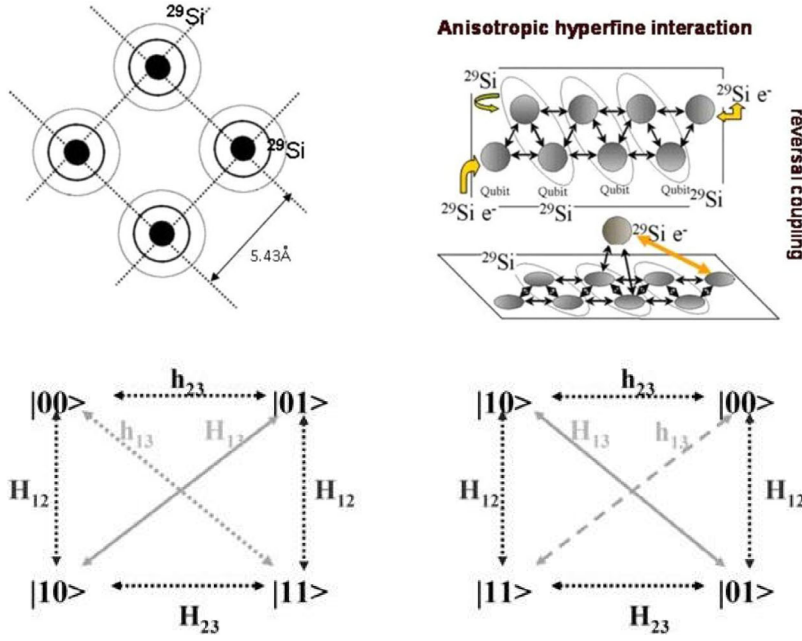


Fig. 1. Top: (left) $\langle 100 \rangle$ representation of the axial channel formed by the four ^{29}Si atoms, where transversal thickness of the target corresponds to one atomic layer, a schematic view. Right: the hyperfine interaction mechanism, a schematic representation. The anisotropic hyperfine coupling yields the synchronization between selective rotations of the adjacent nuclear ^{29}Si spins affected by the circularly polarized electron spin. Bottom: asymmetry measure of the exchange interaction between coupled electron qubit states, a schematic representation. Left: symmetric exchange interaction (indicated by grey full line): $H_{ij} = J(s_{x,i}s_{x,j} + s_{y,i}s_{y,j}) + K(s_{x,i}s_{y,j} - s_{y,i}s_{x,j})$ couples entangled ^{29}Si electron qubit states $|01\rangle$ and $|10\rangle$. Right: the antisymmetric exchange interaction (indicated by grey dashed line): $h_{ij} = j(s_{x,i}s_{x,j} - s_{y,i}s_{y,j}) + k(s_{x,i}s_{y,j} + s_{y,i}s_{x,j})$ couples the states $|00\rangle$ and $|11\rangle$.

approximation of the Thomas Fermi interaction potential [29,30]

$$U_i(r) = \frac{2Z_1Z_2e^2}{d} \sum_{i=1}^3 \alpha_i K_0 \left(\beta_i \frac{r}{a} \right), \quad (8)$$

where Z_1 and Z_2 are the atomic numbers of the proton and the atom, respectively, e is the electron charge, d is the quantum displacement from the harmonic oscillator ground state, r is the distance between the proton and atomic strings, a_0 is the Bohr radius, $a = [9\pi^2/128Z_2]^{1/3} \cdot a_0$ is the atom screening radius, and K_0 is the zero order modified Bessel function of the second kind with the fitting parameters: $(\alpha_i) = (0.35, 0.55, 0.10)$, $(\beta_i) = (0.30, 1.20, 6.00)$ [31]. The internal-spin-Hamiltonian comprises: nuclear and electron spin qubit, localized in nanosilicon target, as depicted in Fig. 1, and a mediator spin system of channeled protons [36]. The Hamiltonian for the case system, placed in an external magnetic field B_z , is

$$H = \omega_e S_z + \omega_{^1\text{H}} I_z^{^1\text{H}} + \omega_{^{29}\text{Si}} I_z^{^{29}\text{Si}} + S_z \otimes \left[\sum_{n \in \text{Si}, ^1\text{H}} [A_n I_z^n + B_n I_x^n] \right]. \quad (9)$$

The Hamiltonian includes the electron spin component S_z along the direction \hat{z} of the static external field B_0 . The operator of the nuclear spins I^n refers to: hyperchanneled protons (^1H), and the ^{29}Si nuclei (highly isotopically abundant nanocrystal

target contains ^{29}Si with $> 99\%$ purity level). $\omega_e, \omega_{^1\text{H}}$ and $\omega_{^{29}\text{Si}}$ are Zeeman frequencies for electron, ^1H , and ^{29}Si nuclei, respectively. A_n and B_n are coefficients of the hyperfine coupling. Such system possesses the primary orientation dependence from the coefficients of the hyperfine interaction. The nuclear spins, i.e., ^1H and ^{29}Si are affected by the hyperfine anisotropic term BS_zI_x which couples longitudinal component of the electron spin S_z with the transverse component of the nuclear spin I_x . The B_z field corresponds to propagation of the excitation laser impulses. For the atom-cavity experiment we use the field stored in the cavity mode to manipulate charged particles at ideal conditions for separate qubit control. The optically generated states in that sense, are able to be transferred as wave-packets along the transmission line for the multiple-qubit sessions realized in spin network.

Application of a magnetic field along the z -axis induces the spin quantization into eigenstates $|\uparrow\rangle$ and $|\downarrow\rangle$ conditioned via external magnetic field B_z , with eigenvalues $S_z = \pm\hbar/2$. The laser pulse initializes the spin at time $t = 0$ into the superposition $|\psi(t=0)\rangle = (|\uparrow\rangle \pm i|\downarrow\rangle)/\sqrt{2}$ for σ^\pm polarized excitation. The electron spin state then coherently precesses according to $|\psi(t)\rangle = (e^{-i\omega t}|\uparrow\rangle \pm ie^{i\omega t}|\downarrow\rangle)/\sqrt{2}$, where $\omega = g\mu_B B_z/\hbar$ is the Larmor precession frequency, g is the effective electron g factor, μ_B is the Bohr magneton, and \hbar is the reduced Planck constant. The electron spin dynamics as a function of time Δt in terms of applied laser pulse trains t_{ls} is given by

$$0 < \Delta t < t_{ls}, S(\Delta t) = \begin{cases} S_x \cos \omega t, \\ S_y \sin \omega t, \\ S_z. \end{cases}$$

$$\Delta t \geq t_{ls}, S(\Delta t) = \begin{cases} S_y(\cos \phi_{ls} \sin \omega t_{ls} \cos \omega t_1 + \cos \omega t_{ls} \sin \omega t_1) - S_z \sin \phi_{ls} \cos \omega t_1, \\ S_y(-\cos \phi_{ls} \sin \omega t_{ls} \sin \omega t_1 + \cos \omega t_{ls} \cos \omega t_1) - S_z \sin \phi_{ls} \sin \omega t_1, \\ S_y \sin \phi_{ls} \sin \omega t_{ls} + S_z \cos \phi_{ls}, \end{cases} \quad (10)$$

where (S_x, S_y, S_z) is the initial spin state, time period is $t_1 = t - t_{ls}$, ω is the precession frequency about the z axis, and ϕ_{ls} is the spin precession angle induced by laser pulse. Focusing the proton beam over the electron spin manifold under angle $\varphi \ll \psi_c$ where ψ_c is critical angle for channeling, induces the switching mechanism in the Hamiltonian of Eq. (9) into two substates:

$$H_1 = \omega_I I_z + S_z (A_n I_z + B_n I_x), \quad H_2 = \omega_I I_z - S_z (A_n I_z + B_n I_x), \quad (11)$$

where a sequence of time delays τ_i and π flips: $\tau_1 - \pi - \tau_2 - \dots - \tau_n - \pi, i = 1, \dots, n$, forms the specific rotations of the nuclear spin in electron spin manifolds, encoded in evolution of the Hamiltonians 1 and 2 (see Eq. (11)) as: $e^{-(iH_2\tau_{2i})} = e^{-(i\pi S_y)} e^{-(iH_1\tau_{2i+1})} e^{-(i\pi S_y)}$ and $e^{-(iH_1\tau_{2i+1})} = e^{-(i\pi S_x)} e^{-(iH_1\tau_{2i})} e^{-(i\pi S_x)}$, respectively. The multiscale time dynamics is implemented into latter sequence which serves as a building block, executing $n\pi$ pulses for every $2\tau_i$ time delays, after applying initial phase shift of the first π pulse by 90 degrees, resulting in the Meiboom-Gill pulse sequence (see Fig. 2). Consequently, the system's evolution $|\psi(t)\rangle = \hat{U}(t)|\psi(t=0)\rangle$ is described by the decomposition of the response function $u'(t)$ [38] figuring in evolution operator, $\hat{U}(t) = u'(t)e^{-i\omega\tau S_z}$, where $u'(t) = \sum_{i=0}^{\infty} u^{2\tau_i} + \sum_{i=0}^{\infty} u^{2\tau_i+1} = \sum_{i=0}^{\infty} \begin{pmatrix} u_{11}^{2\tau_i} & 0 \\ 0 & u_{22}^{2\tau_i} \end{pmatrix} + \sum_{i=0}^{\infty} \begin{pmatrix} 0 & u_{12}^{2\tau_i+1} \\ u_{21}^{2\tau_i+1} & 0 \end{pmatrix}$ includes diagonal, S_z , and antidiagonal, S_x and S_y , components, respectively.

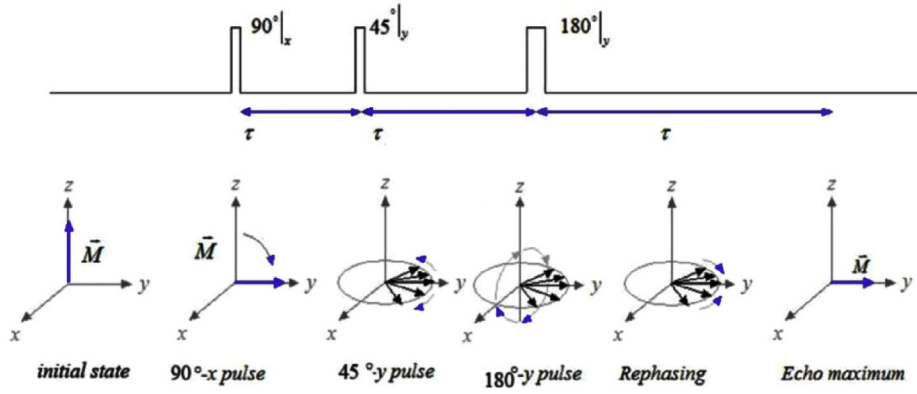


Fig. 2. Selective control of the pulse sequence on the anisotropic hyperfine transition: within a time delay $\tau = \pi/\omega$ for the input pulse of 10% ψ_c at $B_z = 2\text{T}$ which demonstrates coherent exchange interaction between electron and nuclear spins. The electron spin coherence is generated with initial $\pi/2$ pulse, and refocused after the CP pulse $\sim \pi$ as the nuclear spin state is reversibly transferred onto the electron spin: $|\downarrow\rangle \otimes (\alpha|\downarrow\rangle + \beta|\uparrow\rangle) \rightarrow |\uparrow\rangle \otimes (\alpha|\downarrow\rangle + \beta|\uparrow\rangle)$. When the electron is in the triplet, $m_s = 1$ state, the existing hyperfine interaction induces a splitting between the nuclear spin states $\{|1, \downarrow\rangle, |1, \uparrow\rangle\}$. As a result, we can selectively control the nuclear spin state in conjunction with the flip of the electron spin. For a magnetic field $B_z < 0.1\text{T}$, applied perpendicular to the nuclear spin quantization axis, the nuclear spin precesses at the Larmor frequency ω . The hyperfine interaction does not contribute when the electron is in the singlet, $m_s = 0$ state.

The quantum transition between the two adjacent nodes (which represent the coupled system of two ^{29}Si atoms in nanocrystal lattice) and the silicon nanocrystal cavity mode: $|E_c\rangle = \frac{1}{\sqrt{2}}(|e, 0\rangle + |g, 1\rangle)$ in form of resulting quantum state 1-2-C is given by the following relation:

$$|T\rangle = \frac{1}{2} \{ |e_1\rangle (|i_2\rangle + |g_2\rangle) |0\rangle + |g_1\rangle (|i_2\rangle - |g_2\rangle) |1\rangle \}. \quad (12)$$

Here $|T\rangle$ refers to three particle entangled state of $\frac{1}{2}$ spins. The cavity field C coupled with ^{29}Si atoms generates oscillations between the ground $|g, 1\rangle$, excited state $|e, 0\rangle$, and triplet state $|s, 1\rangle$. As a result, the atom-cavity quantum state decay/produce horizontally polarized photons denoted by $|H\rangle$ and vertically polarized photons or $|V\rangle$. It is possible to entangle a stream of such qubits by transmitting them through a thin silicon nanocrystal, exposed to a highly collimated channeled proton beam in order to change the polarization, after the state of the qubits can be read off on exit plane of the crystal. During a read out measurement, a qubit collapse into a 0 or 1 state. Because of the primary orientation-dependable configuration of the triplet states, in addition to polarized beam exposition, tilting of a target additionally allows for the precise control of electron spin manifold with selection of the specific electron triplet state polarization frequency [39]. The laser pulse is used synchronously with a proton beam in this protocol: first in order to drive a well defined superposition of the Zeeman states (given by Eq. (9)) for $B_z = 2\text{T}$ between electron and nuclear spins ($|\uparrow\rangle, |\downarrow\rangle$) in $S-T_+$ qubit basis and, afterward the initialization is performed, in order to control the excitation (driven in $S-T_0$ qubit basis [40]) which corresponds to a mixture of the two electron/nuclear spin states where: $|T_0\rangle \equiv (|\uparrow_e \downarrow_I\rangle + |\downarrow_e \uparrow_I\rangle)/\sqrt{2}$ and $|S\rangle \equiv (|\uparrow_e \downarrow_I\rangle - |\downarrow_e \uparrow_I\rangle)/\sqrt{2}$. Atom-photon entanglement is produced by forming a state with multiple decay channels. Laser ($P = 50 \text{ nW}$) induces the system excitation

in one of the 3P states, imprinting the effective spin coupling states onto a photon, thus allowing the decay through the $P-D^0$ channel via photon $|V\rangle$ which is polarized parallel to the electron-nuclear quantization axis, and photon $|H\rangle$ which is polarized perpendicularly to electron-nuclear quantization axis. A short proton pulses thus provide a direct selective spin control by flipping the state of the excitation selectively in a picosecond time scale ~ 12 ps length. A transition from the systems singlet to triplet state is provided by controlled π pulse rotation relative to selected spin precession angle $\phi_{ts} = J(\varepsilon)/\hbar \leq \psi_c$, which is associated to quantization z -axis. $J(\varepsilon)$ is the exchange coupling between different energy ε sublevels. A proton-probe laser controls the precession over ϑ -angle (relative to $\langle 100 \rangle$ low index axis of a silicon nanocrystal) by the ellipticity which is equivalent to the electron spin polarization. The one dimensional thermal vibration amplitude of the nanocrystal atoms is 0.0074 nm [9, 31] and the average frequency of transverse motion of protons moving close to the channel axis is equal to 5.94×10^{13} Hz. The majorization protocol is performed over two-level system defined by Eq. (9) over subsystems A, B spanning $V \subset H_A \otimes H_B$ in a form of entangled singlet-triplet subsystems (s, t) as:

$$\begin{aligned} |00\rangle_t &\equiv |0\rangle_A |0\rangle_B, |11\rangle_t \equiv |1\rangle_A |1\rangle_B, |10\rangle_{s,t} \equiv |1\rangle_A |0\rangle_B, |01\rangle_{s,t} \equiv |0\rangle_A |1\rangle_B, \\ |\Psi_{\pm}\rangle &= \frac{1}{\sqrt{2}} (|0\rangle_A |1\rangle_B \pm |1\rangle_A |0\rangle_B), |\Phi_{\pm}\rangle = \frac{1}{\sqrt{2}} (|0\rangle_A |0\rangle_B \pm |1\rangle_A |1\rangle_B). \end{aligned} \quad (13)$$

Such subsystems are represented by the coherent mixtures of basis states that form an equal incoherent mixture of the four Bells entangled states $|\Psi_{\pm}\rangle$ and $|\Phi_{\pm}\rangle$ of Eq. (13) (governed by the exchange Hamiltonian $H_{(exch)} = -2JS_1S_2$, where S_1 and S_2 are electron spins associated with ${}^{29}\text{Si}$ nuclei over subsystems A and B). The resonance field and magnitude of the hyperfine transition depend on latter exchange-interaction part of the effective Hamiltonian, as represented in Fig. 3, and on the coupling coefficient B_n (Eq. (9)), respectively. The qubit representation: $|m_S m_I\rangle = |00\rangle, |01\rangle, |10\rangle, |11\rangle$ corresponds to Zeeman product states: $|m_S m_I\rangle = |\uparrow\uparrow\rangle, |\uparrow\downarrow\rangle, |\downarrow\uparrow\rangle, |\downarrow\downarrow\rangle$, where the electron/nuclear spin states are denoted as: $\uparrow = 1/2, \downarrow = -1/2$.

In order to address the atom-photon entanglement we have used the protocol which simultaneously increases both purity and entanglement, at the cost of decreasing the ensemble size of initial photon pairs. In addition, we have theoretically explored the region of maximally entangled Werner state corresponding to generated atom-photon entangled systems. The entangled state is given by: $\hat{\rho}_w = (1-p)\frac{1}{4}\hat{1}_4 + p|\Phi_{\pm}\rangle\langle\Phi_{\pm}|$ where $\hat{1}_4$ denotes the identity matrix, and $|\Phi_{\pm}\rangle = \frac{1}{\sqrt{2}}(|HH\rangle \pm e^{i\varphi}|VV\rangle)$. Here $|HH\rangle$ represents two horizontally polarized, and $|VV\rangle$ denotes two vertically polarized photons. φ corresponds to proton beam incident angle [9, 35]. We have performed superoperator tomography of the density matrix states (16×16) to show the probabilities for the concurrence which refers to Werner entangled states, see Fig. 4.

3.1 Experimental protocol

The entanglement properties of nuclear ${}^{29}\text{Si}$ qubits, which belong to each pair of adjacent nanosilicon sites, are established by exposing the system to synchronized Ti: sapphire ultrafast laser at 82 MHz repetition frequency, in conjunction to 2 MeV energy channeled proton beam pulses, tilted relative to quantization axis by angles: $\varphi = 0.05\psi_c, \varphi = 0.15\psi_c, \varphi = 0.20\psi_c, \varphi = 0.25\psi_c$. The excitation pulses are chosen to match the limits of the Bohr radius, denoted with peak at 20% of the critical angle

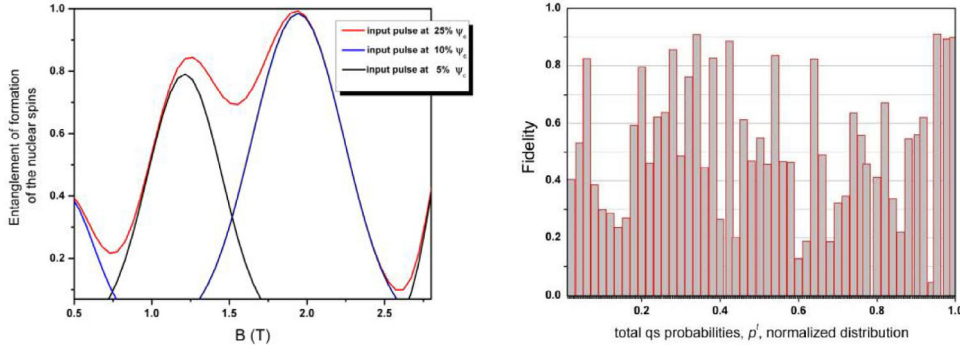


Fig. 3. Left: numerically obtained dependence of the quantity measure of established mixed state entanglement for nuclear spins – entanglement of formation [23] as a function of the implemented magnetic field, considering various channeled proton beam angles. Distribution of amplitudes is obtained from 2 MeV proton beam source with a 92 nm ^{29}Si target for the specified tilt angles: $\varphi = 0.05\psi_c$, $\varphi = 0.10\psi_c$, and $\varphi = 0.25\psi_c$ in the transverse phase plane (according to input pulses at $5\%\psi_c$, $10\%\psi_c$ and $25\%\psi_c$, respectively). The proton beam focusing spot covers the area in the vicinity of the nanocrystal low index $\langle 100 \rangle$ axis and allows the control for two-qubit entanglement with inhibition of the new spin polarizations for the nuclear ^{29}Si spins in adjacent sites. Right: the Uhlmann-fidelity [43] corresponding to mean values and standard deviations obtained from data shots of 10000 quantum Monte-Carlo iterations, each using the quantum state reconstruction of (Eq. (14)).

for channeling ψ_c (relative to tensor principal axis). The anisotropic hyperfine coupling between the triplet state of (^1H mediated) polarized electron spin and the ^{29}Si nuclear spin is further coherently manipulated via selective proton beam pulses where the spins precess under a modified Meiboom-Gill echo sequence [41]. The pulses are generated periodically; picosecond phase interval is indicated in Fig. 2 (at the end of the sequence, the sign of the pulses reverses in order to compensate the accumulation of the phase noise). Entangled photon pairs are generated via spontaneous Stokes Raman transition at the corresponding nanocrystal site with different polarization states $|H\rangle$ and $|V\rangle$. The atom (site) excitation is provided with femtosecond σ^+ polarized pulse, resulting in spontaneous emission to a legible exit state: either 1 or 0, in addition to emission of a photon in $|H\rangle$ or $|V\rangle$ polarization state. By using the polarization beam splitter it is possible then to reflect the photons with polarization $|V\rangle|-\rangle$ and to transmit the photons of polarization $|H\rangle|+\rangle$. The probe laser performs initialization of the atomic qubits into coherent states: $|\psi_1\rangle$ and $|\psi_2\rangle$, which result in the unnormalized two level entangled state between two photon states and two atomic states as: $|\Phi\rangle = \frac{1}{2} [\psi_{2+} |\psi_1\rangle \otimes |\psi_2\rangle_+ - i\psi_{2-} |-\psi_1\rangle \otimes |\psi_2\rangle_-]$ with $|\psi_2\rangle_{\pm}$ denoting the even and odd coherent superposition states:

$$|\psi_2\rangle_{\pm} = \frac{1}{\psi_{2\pm}} (|\psi_2\rangle \pm |-\psi_2\rangle), \psi_{2\pm} = \sqrt{2(1 \pm e^{-2|\psi_2|^2})}. \quad (14)$$

To coherently drive the quantum transition $S \leftrightarrow T_0 \leftrightarrow T_{\pm}$ between $|\psi_1\rangle$ and $|\psi_2\rangle$ states, a laser with $20 \mu\text{eV}$ bandwidth in a pulsed regime is used to generate approximately 150 fs pulse width, much less than the corresponding single-triplet splitting. A full 16×16 Hermitian matrix, obtained from the superoperator tomography [42], is further included in quantum Monte Carlo simulation. Its diagonal elements represent

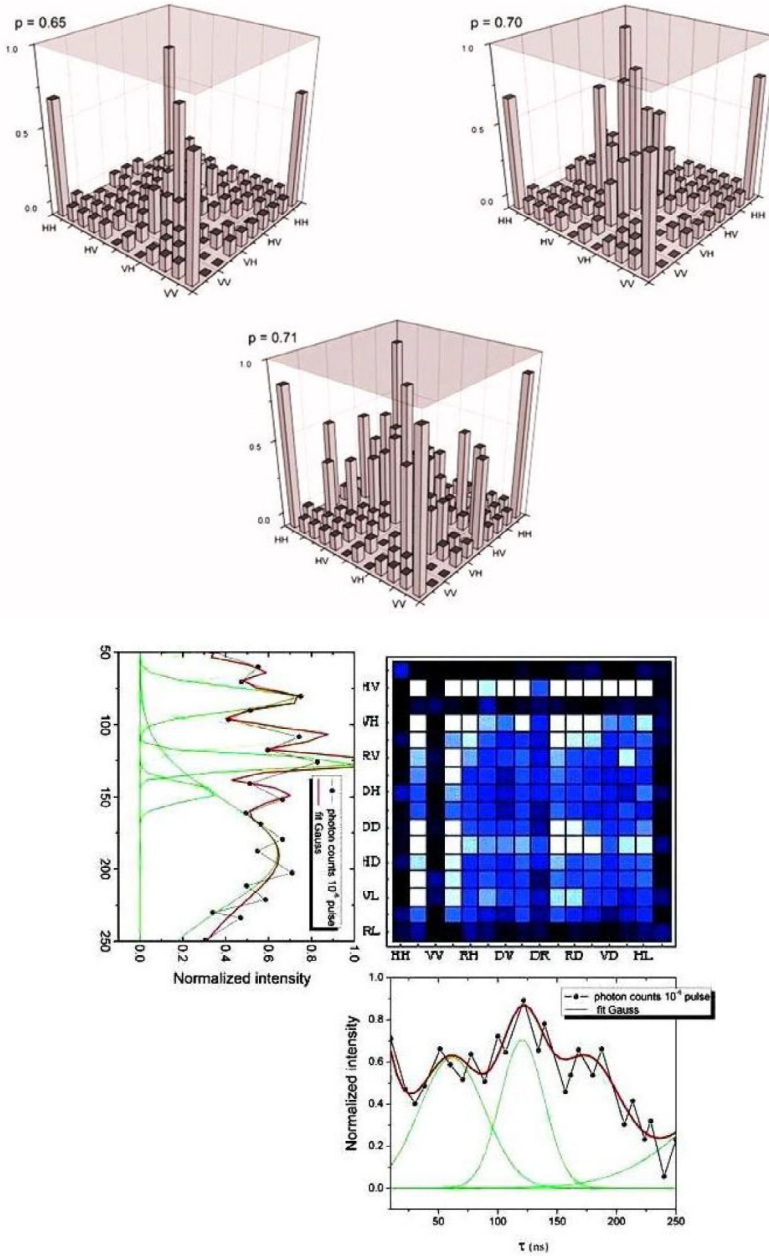


Fig. 4. Top: numerical simulation results for the superoperator real components of Werner states in probability range corresponding to vicinity of $p \leq 1/\sqrt{2}$; imaginary components are omitted. Plots: $p = 0.65$, $p = 0.70$, and $p = 0.71$ correspond to the ion beam incident angle at $\varphi = 0.1\psi_c$, where $\psi_c = [2Z_1Z_2e^2/(dE)]^{1/2} = 6.09$ mrad. Silicon nanocrystal is tilted along the θ_x axis corresponding to the limit $p > 1/3$ which defines the maximal quantity of entanglement. Bottom: quantum Monte-Carlo simulation of two photon count-down emission probability vs noise, as a read out of $m_S = 0$ and $m_S = \pm 1$ states, representing a function of the time delay interval τ_i during a pulse sequence in $x - y$ plane responsible for the corresponding hyperfine transition. Probabilities are obtained using a superoperator density matrix tomography for 16 polarization states corresponding to the matrix elements of Eq. (15).

a linear combination of different coincidence measurements, where:

$$\begin{bmatrix} |H\rangle_1 \otimes |H\rangle_2 & |R\rangle_1 \otimes |H\rangle_2 & |D\rangle_1 \otimes |R\rangle_2 & |V\rangle_1 \otimes |D\rangle_2 \\ |H\rangle_1 \otimes |V\rangle_2 & |R\rangle_1 \otimes |V\rangle_2 & |D\rangle_1 \otimes |D\rangle_2 & |V\rangle_1 \otimes |L\rangle_2 \\ |V\rangle_1 \otimes |V\rangle_2 & |D\rangle_1 \otimes |V\rangle_2 & |R\rangle_1 \otimes |D\rangle_2 & |H\rangle_1 \otimes |L\rangle_2 \\ |V\rangle_1 \otimes |H\rangle_2 & |D\rangle_1 \otimes |H\rangle_2 & |H\rangle_1 \otimes |D\rangle_2 & |R\rangle_1 \otimes |L\rangle_2 \end{bmatrix}, \quad (15)$$

where: $|D\rangle = \frac{|H\rangle+|V\rangle}{\sqrt{2}}$, $|L\rangle = \frac{|H\rangle+i|V\rangle}{\sqrt{2}}$, and $|R\rangle = \frac{|H\rangle-i|V\rangle}{\sqrt{2}}$.

Figure 3 represents the fidelity, F , of an obtained set of state $\psi_{2\pm}$ tomography data (given in Fig. 4), expressed by:

$$F(\psi_{2\pm}) = \sum_{\rho} p^t F(\rho, \psi_{2\pm}). \quad (16)$$

The corresponding discrepancies, ΔF , with respect to a desired state $\psi_{2\pm}$ (see Eq. (14)) are obtained as: $\Delta F(\psi_{2\pm}) = \sum_{\rho} p^t \left((F(\rho, \psi_{2\pm}) - F(\psi_{2\pm}))^2 \right)^{1/2}$. Considering N iterations to detect f_i results from probability distribution function given by: $f(p, c, N) = \prod_j \frac{p \cdot D_p(c_j m_k) + (1-p) \cdot D_p(c_j m_l)}{D_p(c_j m_k) + D_p(c_j m_l)}$, where $D_p(c_j m_{\{k,l\}}) = \frac{m_{\{k,l\}}^{c_j} e^{-m_{\{k,l\}}}}{c_j!}$ represents the normalized probabilities of detecting c_j counts for a given Poisson distribution centered around mean values for $m_{\{k,l\}}$ and $m_S = 0$ and $m_S = \pm 1$ states, one can obtain the binomial distribution of a probability distribution function $f(p, c, N)$. Here the total probability p^t , of a quantum state $\psi_{2\pm}$ in measurement process is given by the product of all probabilities as: $p^t = \frac{\prod_i f(\text{Tr}(P_i \rho), n_i, N)}{\sum_{\rho} \prod_i f(\text{Tr}(P_i \rho), n_i, N)}$. In this way for each iteration one can utilize series of continual deterministic measurements which are non-destructive [44] with respect to the entangled atom-photon state, establishing a quantum feedback control of a solid state qubit through its integrated dynamical correlation with CP induced EM field.

4 Summary

We have demonstrated asymmetric coupling mechanism and precise control of proton beam induced atom-photon quantum correlations for QED-based entanglement in channeling regime and described conversion protocol which efficiently maps the channeled ion into atom-photon quantum state, allowing the efficient generation of entangled state between arbitrary localized spatial centers in silicon matrix. Coherent control is utilized through spin precession in the proton exchange field which is initialized via 2 MeV energy proton beam pulses. The noise reduction through the correlation process is achieved by establishing the specific circumstances when two quantum objects – spin qubits form a unique mixed quantum state in the composite system, type: singlet – triplet. In that context, the process of coupling of electron with 1/2 nuclear quantum spin states in silicon nanocrystal target, mediated by the polarized nuclear spin states of channeled protons through the quantum entanglement, allows the transfer of information originally deposited in the electrons to the spin state of the host ^{29}Si . The resulting transfer of quantum information in long-lived quantum state (polarization) of a nuclear spin is further addressable to a photon, with corresponding polarization/frequency applying the quantum feedback control strategy. Obtained results support further investigation toward ion-beam manipulation

of hybrid spin states, emphasizing the correlated quantum state transfer in higher dimensional systems states over the spin network.

Author acknowledges the grant ObAd: 1007211, and support from the Ministry of Science and Education.

References

1. D. Heiss (ed.), *Fundamentals of Quantum Information* (Springer, New York, 2002)
2. C.H. Bennett, et al., *Phys. Rev. Lett.* **70**, 1895 (1993)
3. B. Blinov, D.L. Moehring, L.M. Duan, C. Monroe, *Nature* **428**, 153 (2004)
4. T. Wilk, S.C. Webster, A. Kuhn, G. Rempe, *Science* **317**, 488 (2007)
5. J. Sherson, et al., *Nature* **443**, 557 (2006)
6. H.J. Kimble, *Nature* **453**, 1023 (2008)
7. M. Horodecki, P. Horodecki, R. Horodecki, in *Quantum Information: An Introduction to Basic Theoretical Concepts and Experiments*, Vol. 173 of Springer Tracts in Modern Physics, edited by G. Alber, et al. (Springer Verlag, Berlin, 2001), p. 151
8. A.D. Boozer, et al., *Phys. Rev. Lett.* **98**, 193601 (2007)
9. V. Berec, *PLoS ONE* **7**(9), e45254 (2012)
10. V. Filidou, et al., *Nature Phys.* **8**, 596 (2012)
11. S.K. Gorman, M.A. Broome, W.J. Baker, M.Y. Simmons, *Phys. Rev. B* **92**, 125413 (2015)
12. A. Fang, Y.-C. Chang, J.R. Tucker, *Phys. Rev. B* **72**, 075355 (2005)
13. C.D. Hill, et al., *Sci. Adv.* **1**, e1500707 (2015)
14. Z. Kurucz, et al., *Phys. Rev. Lett.* **103**(1), 010502 (2009)
15. H. Wiseman, *Phys. Rev. A* **49**, 21332150 (1994)
16. D. Liberzon, *Switching in Systems and Control* (Birkhauser, Boston, 2003)
17. B. Gopalakrishnan, et al., *Nature Mater.* **8**(5), 383 (2009)
18. J.J. Morton, B.W. Lovett, *Ann. Rev. Cond. Matt. Phys.* **2**, 189 (2011)
19. J.S. Hodges, J.C. Yang, C. Ramanathan, D.G. Cory, *Phys. Rev. A* **78**(1), (2008) 010303
20. G.W. Morley, et al., *Phys. Rev. Lett.* **98**(22), 220501 (2007)
21. S.A. Lee, W.M. Jr. Fairbank, *Phys. Rev. A* **82**(4), 042515 (2010)
22. T.D. Ladd, D. Maryenko, Y. Yamamoto, E. Abe, K.M. Itoh, *Phys. Rev. B* **71**, 01440 (2005)
23. P. Buek, V. Rungta, C. Caves, M.M. Hillery, G.J. Milburn, *Phys. Rev. A* **64**, 042315 (2001)
24. W.K. Wootters, *Phys. Rev. Lett.* **80**, 2245 (1998)
25. M. Horodecki, P. Horodecki, R. Horodecki, *Phys. Rev. Lett.* **80**, 5239 (1998)
26. T.C. Wei, P.M. Goldbart, *Phys. Rev. A* **68**, 042307 (2003)
27. A. Mann, B.C. Sanders, W. Munro, *Phys. Rev. A* **51**, 989 (1995)
28. C.A. Fuchs, *Phys. Rev. Lett.* **79**, 1162 (1997)
29. S. Hill, W.K. Wootters, *Phys. Rev. Lett.* **78**, 5022 (1997)
30. C.M. Caves, C.A. Fuchs, P. Rungta, *Found. Phys. Lett.* **14**(3), 199 (2001)
31. W.K. Wootters, *Quant. Inf. Comput.* **1**(1), 27 (2001)
32. W.J. Munro, D.F.V. James, A.G. White, P.G. Kwiat, *Phys. Rev. A* **64**, 030302 (2001)
33. R.F. Werner, *Phys. Rev. A* **40**, 4277 (1989)
34. D.S. Gemmell, *Rev. Mod. Phys.* **46**, 129 (1974)
35. S.L. Chang, et al., *Phys. Rev. Lett.* **94**, 174801 (2005)
36. K.D. Liss, et al., *Nature* **404**(6776), 371 (2000)
37. E. Tsyganov, A. Taratin, *Nucl. Instr. Meth. Phys. Res. A* **363**, 511 (1995)
38. M. Motapothula, et al., *Phys. Rev. Lett.* **108**, 195502 (2012)
39. V. Berec, *Laser Part. Beams* **33**(01), 1 (2015)
40. V. Berec, et al., *Nucl. Instr. Meth. B* **355**, 324 (2015)
41. A. Castro, I.V. Tokatly, *Phys. Rev A* **84**, 033410 (2011)

42. X. Wang, L. Bishop, S. Kestner, J.P. Barnes, E.K. Sun, S.S. Das, *Nat. Commun.* **3**, 997 (2012)
43. H. Bluhm, et al., *Nature Phys.* **7**(2), 109 (2010)
44. P.T. Callaghan, *Principles of Nuclear Magnetic Resonance Microscopy* (Oxford: Clarendon Press, 1993)
45. U. Leonhardt, H. Paul, G.M.D. Ariano, *Phys. Rev. A* **52**, 6 (1995)
46. A. Uhlmann, *Rep. Math. Phys.* **9**, 273 (1976)
47. G.G. Gillett, et al., *Phys. Rev. Lett.* **104**, 080503 (2010)